Title: Effect of machining parameters and cutting tool coating on hole quality in dry drilling of fibre metal laminates

Authors:

K. Giasin*[a], G. Gorey [a], C. Byrne[a], J. Sinke[b], E. Brousseau[a]

[a] School of Engineering, Cardiff University, Cardiff, CF24 3AA, UK

[b] Kluyverweg 1, 2629 HS Delft, Delft University, Netherlands.

*Corresponding author: giasink@Cardiff.ac.uk, Tel: +44 7542 138643

Abstract

Fibre metal laminates (FMLs) are a special type of hybrid materials, which consist of sheets of metallic alloys and prepregs of composite layers stacked together in an alternating sequence and bonded together either mechanically using micro hooks or thermally using adhesive epoxies. The present paper contributes to the current literature by studying the effects of three types of cutting tool coatings namely TiAlN, AlTiN/TiAlN and TiN on the surface roughness and burr formation of holes drilled in an FML commercially known as GLARE®. While the cutting tool geometry is fixed, the study is also conducted for a range of drilling conditions by varying the spindle speed and the feed rate. The obtained results indicate that the spindle speed and the type of cutting tool coating had the most significant influence on the achieved surface roughness metrics, while tool coating had the most significant effect on burr height and burr root thickness. The most important outcome for practitioners is that the best results in terms of minimum roughness and burr formation were obtained for the TiN coated drills. However, such drills outperform the other two types of tools, i.e. with TiAlN and AlTiN/TiAlN coatings, only when used for short series of hole drilling due to rapid tool deterioration.

Keywords: Drilling; GLARE; Surface roughness; Burr formation; Coating.

1. Introduction

Fibre metal laminates (FMLs) are hybrid materials made up of alternating layers of thin metallic sheets and composite layers. The metal sheets and composite layers are bonded together either mechanically, using micro hooks produced on the surfaces of the metallic sheets, or thermally, using adhesive epoxies. FMLs are composed of metals such as aluminium and either of glass (commercially known as GLARE®) based on R-glass or S2-glass fibres, Aramid (commercially known as ARALL®) or carbon (commercially known as CARALL®) [1]. Applications for FMLs are consistently growing, particularly in the aerospace and defence sectors due to their high performance [2, 3]. FMLs which contain aluminium alloys such as GLARE® and ARALL® were mainly developed for aircraft components where fatigue resistance is needed such as in the lower wing and fuselage skins of a plane [3]. Recently, GLARE® laminates were also tested for potential spacecraft shielding applications to assess their efficiency in the outer space against debris undergoing hypervelocity impacts of multiple kilometres per second. The first commercial aircraft to use GLARE® in its structure was the Airbus A380 [3, 4]. 25% of the A380 airframe is made of composites, 22% of which are carbon or glass fibre reinforced plastics CFRPs and 3% GLARE® [3, 5]. GLARE® is used in the front fairing, upper fuselage shells, crown and side panels, and the upper sections of the forward and aft upper fuselage [6]. For example, the Airbus A380 has two large sections of GLARE (approx. 400 m^2): one in front of the main wing covering the side panels and the crown panel; and one section after the main wing. Next the leading edge for the vertical tail plane is also made of GLARE for bird-impact resistance. GLARE® structures are usually produced in large panels of more than 2 metres (the panels can be as large as 3 x 10 meters) and machining is required to bring those panels into the desired dimensional requirements and also, to prepare them for assembly [1-3, 7]. The machining of GLARE® is carried out by conventional and non-conventional material removal methods [1-3]. The conventional methods most frequently

employed are edge milling and drilling, while the non-conventional machining processes include abrasive waterjet and laser cutting [1, 7]. For non-conventional methods, it was found that waterjet cutting can be used for pre-cutting (not finishing operations); while laser jet cutting is not used because of deterioration of edge quality due to high temperatures [1, 7].

Holes are drilled into GLARE® panels to join them together using mechanical fasteners and rivets, while edge milling is used to give the panels the desired contour shapes for mating purposes [7]. Building a modern aircraft involves numerous manufacturing steps, including creating holes to accommodate the fasteners required to complete assembly components and sub-assemblies of a wing or a section of the fuselage. Indeed, riveting is the most common joining process in aircraft manufacturing [8]. Riveting can be challenging especially when holes are produced in large scales. For example, an Airbus A380 wing contains 32,000 major parts, excluding fasteners, held together by 750,000 bolts and rivets to join various aircraft components to configure the final structure. 180,000 holes are drilled in a single Airbus 380 wing box alone [9]. It is estimated that 60% of all part rejections is due to poor hole quality [10]. Therefore, a suitable selection of cutting parameters, cutting tool coating and geometry must be chosen when drilling hybrid metal composite materials to minimise any defects in both materials. In addition, it is vital that the holes are chamfered and free of metal burrs to reduce post machining deburring for proper assembly and thereby increasing productivity and keep tool costs to a minimum.

The challenges in machining GLARE® arise from its hybrid structure which differs in many aspects from machining metals or composites individually. It was previously reported that good hole quality in GLARE® can be achieved with no delamination or deformation using the proper speed/feed ratios and proper drill bits [1, 3]. Twist drills are the most commonly used tools in drilling operations for joining and assembly operations [11, 12]. Cutting tools made from hard materials are recommended for drilling GLARE® on CNC machines [3]. The cutting tool

should be capable of withstanding the abrasiveness of glass fibres and have a low tendency for chip adhesion and built-up edge to improve the borehole surface quality. There has been a steady rise in studies carried out on the machinability of GLARE® laminates in the past few years [2, 3, 13-23] as shown in Table 1. Essentially, these studies investigated the influence of cutting parameters and cutting tool geometry on the surface finish of machined holes. Previous tests on different cutting tools materials showed that polycrystalline diamond PCD and solid cemented carbide drills with coatings are most suitable for machining GLARE® [1, 3, 13]. Whereas coated and uncoated high-speed steel HSS tools rapidly wear due to the high hardness of S2 glass fibres [1, 3]. The selection of cutting speeds and feed rates depend on the mechanical properties of the workpiece, the type of material used for the drill bit and its coating. Previous researchers used HSS and carbide cutting tools to drill aluminium and its alloys [24-27] and they found that both were suitable for drilling aluminium. Carbide and coated tools outperformed the non-coated and HSS tools in terms of tool wear and hole quality when drilling aluminium alloys, GLARE® and composite-metal stacks [3, 25, 26, 28]. However, none of the previous studies reported the impact of cutting tool coatings on hole quality in GLARE® laminates using a fixed cutting tool geometry (i.e. size, point angle and helix angle). Thus, using different tools with the same geometry and base material, i.e. tungsten carbide, but with different coatings, the aim of this work is to fill this gap. In particular, the study reported here evaluated the impact of the spindle speed (n), the feed rate (f) and three types of cutting tool coatings, namely TiAlN, TiN and AlTiN/TiAlN on hole roughness parameters (R_a and R_z) and burr formation (burr height and burr root thickness) in the first and last aluminium sheets in GLARE® 2B11/10 laminates. The drilling experiments were designed based on a full factorial model and the results were further analysed using the ANOVA (Analysis of Variance) statistical technique to determine the contribution of each input parameters and their linear interactions on the output parameters.

2. Materials and methods

2.1 Workpiece and cutting tools

This investigation considered one grade of GLARE® 2B 11/10-0.4 laminate as shown in Fig.1(a) The laminate was supplied by the Fibre-Metal Laminate Centre of Competence (FMLC) in the Netherlands. The distance between the centre of each two adjacent hole was kept constant at 12 mm as shown in Fig.1(b). This distance was fixed to ease the drilling process using the CNC machine and the post machining measurements. The 12 mm distance was also chosen to minimise the impact on the drilled hole from the adjacent holes in the workpiece. The workpiece consisted of thin sheets of Al2024-T3 alloy having a nominal thickness of 0.4 mm and prepregs of S2-glass fibres embedded with FM94 adhesive having an approximate thickness of 0.133 mm [1, 2, 16, 20, 21]. The aluminium sheet surfaces were pre-treated and degreased followed by chromic acid anodising and subsequent priming with BR-127 corrosion inhibiting bond primer. The fibres were delivered as a prepreg including the FM94 adhesive system from Cytec in the U.K [1]. Each glass fibre layer consisted of two unidirectional prepregs oriented at [90°/90°] as shown in Fig.1(c), where the rolling direction in aluminium sheets is defined as (0°). The dimensions of the GLARE® panel used in this study were 200 x 150 x 7.13 mm. Finally, the sample was cured in an autoclave for around 300 minutes at elevated temperatures of 120°C and under a pressure of 6 bars [29].

The cutting tools considered in this work were all Ø6 mm coated carbide twist drills with a point angle of 140° and a helix angle of 30° as shown in Fig.2. The choice of cutting tool geometry and coatings was based on previous literature [1-3, 14, 15]. The standard helix angle for most drills is 30° [30], despite the fact that most drills come with a 118° drill point angle, when it comes to drilling composites it is recommended to use a drill bit with a 135° point angle [11]. Similarly for drilling aluminium, recommended point angles for drilling Al2024

alloys are in the range 130°-140° [2, 31, 32]. In addition, a cutting tool with large helix angle - usually larger than 24°- flutes allowing quick chip evacuation [3, 32, 33], while large point angles improve chip removal and reduce burr formation. For drilling aluminium alloys, the drill point angle to be used depends on the silicon content in the workpiece. For aluminium alloys with low or no silicon content, a 130°-140° point angle is recommended [3, 31, 32]. It was also reported that the surface roughness is affected by the point and helix angles such that increasing these two parameters can minimise roughness and burr formation [34, 35]. Moreover, the Ø6 mm drill bit was chosen since it is a common size for creating rivets and holes in aerospace structures. Most previous drilling studies used a tool diameter between 5-10 mm and holes drilled in Airbus A380 structures range between 4.8-6.4 mm [2, 3, 21].

The coating is a micrometre-thick layer of a specific material applied to the surface of the cutting tool. The functions of the coating are to improve the performance of the cutting tool by extending its life and also to provide better physical and chemical stability at high temperatures thus allowing for higher cutting speeds. The three types of coatings used in this study and the full details of the cutting tools dimensions, geometry and other properties are given in Table 2. Nano-A ™ is a micro-layered coating that combines TiAlN (Titanium Aluminium Nitride) and AlTiN (Aluminium Titanium Nitride) for better heat and wear resistance. The Nano-A coating will be referred to as AlTiN/TiAlN coating hereafter. The micro-layer structure of AlTiN/TiAlN coating makes a better choice for applications for materials with over 45 HRC as reported by the tool supplier. The coating is suitable for high-speed drilling of alloyed steel, stainless steel and aerospace materials. TiN (Titanium Nitride) coating is one of the most popular general-purpose cutting tool coatings. It provides effective protection against abrasive and adhesive wear and has high adhesion and ductility characteristics [36]. It also has good thermal stability and a low coefficient of friction which reduces built-up edge and improves the thermal transfer of heat away from the cutting tool. TiN based cutting tool coatings have

friction reducing property, which shortens the contact length between the tool and chip giving lower torque values during the initial contact of the drilling process [37]. The TiAlN (Titanium Aluminium Nitride) coating is suitable for dry machining applications, it has good ductility and improved oxidation resistance and hardness compared to TiN [36-38]. Generally, TiN TiAlN and AlTiN coatings are common for rotary tooling such as drilling [36].

The experiments conducted in this work combined three spindle speeds, three feed rates and three types of cutting tool coatings. To confirm the repeatability of the study, each combination of experimental parameters was repeated two additional times and the mean values of the three results were reported. The study employed a full factorial design with three factors (i.e. spindle speed, feed rate and tool coating) at three levels each to detect the influence of these input parameters on measured outputs, which were surface roughness and burr formation metrics. Table 3 summarises the cutting parameters used in the experiment. The results were analysed using ANOVA via the MINITAB®18 software to test the significance of each factor and their interaction, the percentage contribution of cutting parameters, cutting tool coatings and their interactions on roughness and burr metrics are provided in Table 4 and Table 5.

The values of (Prob>F-value) less than 0.05 in ANOVA tables means that the effect of the model, the factors (spindle speed, feed rate, coating) and their interactions on the response parameters (R_a, R_z, burr height and bur root thickness) are significant at 95 % confidence level. Here, F-value is the ratio of two variances (variance is the square of the standard deviation). Variance is a measure of dispersion, or how far the data are scattered from the mean. Larger F-values represent greater dispersion [39]. An F-value is reported for each test in the analysis of variance table. Minitab uses the F-value to calculate the p-value, which is used to assess the statistical significance of a given parameter or a combination of parameters [39].

Each set of nine holes combining three spindle speeds and three feed rates was drilled with a new tool to minimize any effect of tool wear, adhesions or build up edge (BUE) [32] and no coolants were used in this study. The cutting parameters were selected according to previous literature on machining FMLs and based on recommendations of tool manufacturers. Existing literature indicates that the feed rate used for drilling GLARE®/FMLs, composite metal stacks, aluminium alloys and glass fibre reinforced plastics (GFRP) ranged between 0.05 to 0.3 mm/rev, while the spindle speeds - depending on the size of the cutting tool - ranged between 1000 to 9000 rpm [2, 3, 14-16, 18, 23, 40-42].

2.2 Experimental machine setup and procedure

Drilling experiments were conducted on a Geo Kingsbury - CNC milling machine, which could provide spindle speeds of up to 6000 rpm. The machining operations were programmed using a GE Series Fanuc 0-MC controller. The GLARE® sample was mounted and bolted on a specially designed stainless-steel support plate with a thickness of 20 mm as illustrated in Fig.3.

2.3 Surface roughness measurements

The quality of the hole surface finish in machined parts can influence their performance and a number of related metrics are usually used as criteria for accepting the finished part [43]. Surface roughness is mainly affected by the machining parameters and drilling tool geometries due to the continuous vibration of the cutting tool. Many metrics have been proposed to describe surface roughness characteristics. Those adopted in this study are 1) the arithmetic average roughness, R_a, which is the arithmetic average height of roughness component irregularities (peak heights and valleys) from the centerline, measured within the sampling length, L as shown in equation 1 and 2) ten-point mean roughness, R_z which is the sum of the average tallest five peaks and the average of five lowest valleys within the sample length as shown in equation 2.

$$R_a = \frac{1}{L}\int_0^L |y(x)|dx \ldots\ldots (1)$$

$$R_z = \frac{|Y_{P1} + Y_{P2} + Y_{P3} + Y_{P4} + Y_{P5}| + |Y_{V1} + Y_{V2} + Y_{V3} + Y_{V4} + Y_{V5}|}{5} \ldots\ldots (2)$$

where:

y(x) is the function describing the profile height, L is the profile length, Y_{P1}, Y_{P2}, Y_{P3}, Y_{P4}, Y_{P5} are the tallest 5 peaks within the sample and Y_{V1}, Y_{V2}, Y_{V3}, Y_{V4}, Y_{V5} are the lowest 5 peaks within the sample.

A Taylor Hobson Talysurf Series 2 surface profilometer was employed for measuring the surface roughness profiles R_a and R_z. The Talymap surface analysis software was used for surface metrology report generation and the analysis of 2D measured profiles. The software was employed for normalizing measurement data and eliminating noise, aberrations or anomalies if any. The MountainsMap premium v7.4 software was used to post-process surface roughness data. A small-bore Taylor Hobson skiddless stylus arm – code 112/2012 was used to measure the roughness parameters. The stylus had a vertical range and resolution of 1.0 mm and 16 nm, respectively. The stylus measurement traverse speed was set at 0.5 mm/sec during the inspection. The stylus arms had a 90˚ coni-sphere diamond stylus with 2 µm nominal radius tip. The stylus arm was connected to a 50 mm inductive traverse unit. The adopted procedure was to measure a total distance of 6.5 mm, which accounted for approximately 90% of the drilled hole depth, similar to previous studies [2, 3]. This was the maximum possible length to measure through the hole depths. The limitation of this method is that the measured surface roughness data is governed by the size of the stylus used, which makes it extremely difficult to detect narrow areas smaller than the stylus tip radius [2, 3]. The surface roughness measurement process is shown in Fig.4(a). The samples were placed such that the holes were facing the stylus from the entrance side and the stylus was inserted into the hole at the maximum possible depth [2, 3]. The stylus was then automatically lowered until it contacted

the hole surface. Then, the stylus traversed along the hole thickness and its profile was recorded [2, 3]. This procedure was repeated 4 times for each hole by rotating the sample 90° along its side to avoid the influence of the fibre direction on the recorded profiles as surface roughness results mainly depends on the stylus path with respect to fibre direction [44]. The R_a and R_z metrics were then extracted by the software for each of the four profiles for a given hole and their mean values from the four readings were automatically calculated. Fig.4(b) shows an example of surface roughness profile for one of the drilled holes in GLARE® 2B 11/10-0.4.

2.4 Burr formation

In this study, the burr formation was characterised by measuring the burr height and the burr root thickness around the edges of the first and last aluminium sheets as reported in previous studies [3, 20, 32]. Measuring the formed burrs is important as this can give an indication of the quality of the drilled hole [3]. Deburring operations can account for about 30% of the total manufacturing cost and can occupy 40% of the total machining time [45, 46]. Even though burr height is the most common measured characteristic for assessing burrs, burr thickness contributes more to deburring costs than burr height [3, 47]. Burr formation is one of the common challenges associated with drilling metals and multi-material stacks as burrs and rough edges on fastener holes can cause stress concentrations, which could initiate fatigue failures, corrosion and reduction in the life of the aircraft [3, 48]. In addition, they can decrease the functionality of components and can cause injuries [49, 50]. The formation of burrs due to the drilling process is shown in Fig.5(a). The burr parameters were defined previously by Schafer [51] and are widely used to characterize burr formation (burr profile shape) in machined holes as shown in Fig.5(b). Both burr parameters were measured with the Taylor Hobson profilometer, which was also employed for measuring the surface roughness. The burr parameters were measured with a recess stylus arm - code 112/2011, the stylus traverse speed

was set at 1 mm/sec. Burr parameters were measured at 0, 90,180 and 270 degrees around the upper- and lower-hole edges, and their average was taken for the final burr value, as shown in Fig.5(c). The locations are named as entrance burr and exit burr throughout the rest of the paper. The stylus was positioned a few millimetres away from the hole edge at the stated locations (0, 90, 180 and 270 degrees around the hole), and was then allowed to move towards the centre of the hole [3, 32]. The stylus recorded the changes along its path while moving towards the centre, thus mapping the burr profile as shown in Fig.5(c). The MountainsMap premium software was used to measure the burr height and burr root thickness profiles.

2.5 Scanning Electron Microscopy (SEM)

A Carl Zeiss 1540 XB field emission Scanning Electron Microscope (SEM) as shown in Fig.6(a). Prior to the SEM inspection, each tool was cut several millimetres below the tip and then cleaned using acetone in an ultrasonic bath for ten minutes to remove any dust or debris on their surfaces. The tools were then placed on the top of a carbon sticker and inserted inside the SEM chamber for surface inspection as shown in Fig.6(b). and Fig.6(c).

3. Results and Discussion

3.1 Surface roughness analysis

The roughness values reported in the current study are a combination of the roughness contributed by both the aluminium sheets and the glass fibre layers when measuring each hole. It was not possible to measure the roughness parameters of the individual FML constituents using the 2D surface profilometer due to the alternating layered structure of the GLARE® panel [2, 3]. However, it could be observed qualitatively that the roughness of the individual aluminium sheets was always smaller than the roughness of the individual glass fibre layers as shown previously in Fig.4. This is due to the heterogeneous nature of composite materials and the effect of fibre orientation relative to the direction of cut [3, 52]. In addition, the fibrous and

brittle nature of glass fibres means that they are prone to fibre pull-out and matrix degradation during the drilling process. This can result in "random" fracture surfaces during cutting leading to higher roughness in the glass fibre layers compared to that observed in the aluminium layers [3, 21]. Besides, voids (pockets) of complete fibre/matrix loss are common when drilling composite/metal stacks partially caused by the evacuated aluminium chips rubbing against the internal surfaces of the hole [3, 52].

Fig.7. and b show the average values for R_a (average surface roughness) and R_z (ten-point mean roughness) of drilled holes under different cutting parameters for the three types of cutting tool coatings used in the study. Overall, R_a ranged between 1.11 and 2 µm while R_z ranged between 9.24 and 16.98 µm. Generally, the highest R_a and R_z values were found when drilling with TiAlN coated tools and these metrics were the lowest when using TiN coated tools. The TiN coating has a slightly lower coefficient of friction than TiAlN and AlTiN coatings, which could have had an beneficial impact on the generated surface roughness [53]. In addition, titanium has a special affinity for aluminium, which means that chemical and physical diffusion processes are triggered especially at the cutting edges under the influence of pressure and heat. This causes aluminium chips to bind into the coating, aluminizing the surface of the drill and increases the friction between the tool and the material increasing roughness of machined holes. Previous studies reported that TiN coated tools produced a similar workpiece roughness to that obtained with TiAlN coated tools when machining CFRP and Al2024-T3 alloy [27, 54]. The different outcome obtained here indicates that the interaction of the GLARE® constituents, and most likely the glass fibre, with the cutting tool coating plays a significant role in determining the quality of hole roughness. It was also observed that the variation of hole roughness between the three tool coatings was small when drilling at spindle speeds of $n = 3000$ and 4500 rpm and was more significant when drilling at the higher spindle speed of $n = 6000$ rpm. The lowest R_a was measured for a hole drilled at $n = 3000$ rpm and $f = 300$ mm/min using TiN coated

tools, and the highest R_a at $n = 6000$ rpm and $n = 300$ mm/min using TiAlN coated tools. The lowest R_z was measured for a hole drilled at $n = 3000$ rpm and $f = 300$ mm/min using TiN coated tools and the highest R_z was at $n = 6000$ rpm and $n = 600$ mm/min using TiAlN coated tools. Generally, R_a increased with the increase in spindle speed regardless of the cutting tool coating. In this case, the increased rubbing of the cutting tool on the drilled hole walls increases the temperatures at the cutting zone, which in return increases the ductility of the laminate constituents and deformations in the hole leading to higher surface roughness. In addition, the increase in surface roughness with the increase in spindle speed could be due to the higher likelihood of ploughing taking place - rather than cutting with chip formation - as the undeformed chip thickness reduces. With respect to the feed rate, its influence varied for different cutting parameters and coatings. For tools with TiN and AlTiN/TiAlN coating, the surface roughness increased with the increase of the feed rate at both $n = 3000$ and $n = 4500$ rpm, while it decreased with the feed rate increase at $n = 6000$ rpm. For TiAlN coating, the surface roughness increased with the feed rate at $n = 3000$, and then it decreased when increasing the feed rate at $n = 4500$ and 6000 rpm. Generally, R_z also increased with the increase in spindle speed regardless of the type of the cutting tool coating. R_z also increased with the increase of the feed rate at all spindle speeds when using AlTiN/TiAlN coated tools, while it increased with the increase of the feed rate only at the spindle speed of $n = 6000$ rpm when using TiAlN coated tools and at spindle speed of $n = 4500$ rpm when using TiN coated tools. At other spindle speeds using TiN and TiAlN coated tools, R_z increased with the increase of the feed rate from $f = 300$ mm/min to $f = 450$ mm/min then decreased with it at $f = 600$ mm/min.

The ANOVA results reported in Table 4 show that the spindle speed and cutting tool coating had significant impact on R_a, contributing by 30.44% and 31.97% respectively, while the feed rate did not have any significant contribution. The two-way interaction between the spindle

speed and the feed rate, and between the spindle speed and the tool coating had some impact on R_a with contributions of 3.98% and 15.98%, respectively. The interaction between the feed rate and tool coating was insignificant, also the three-way interaction between the spindle speed, feed rate and tool coating were insignificant. For R_z, the ANOVA results showed that all three factors considered had significant impact. However, in-line with the outcome obtained for R_a, the spindle speed and the cutting tool coating were the two parameters with the most influence. The two-way interaction between the spindle speed and the feed rate, and between the cutting tool coating and the feed rate were insignificant, while the interaction between the spindle speed and tool coating had a low contribution of 7.58%. The three-way interaction between the spindle speed, feed rate and tool coating also had a minor contribution of 5.22%. Additionally, it was observed that when drilling at a feed rate/spindle speed ratio of 0.1 (mm/min)/rev (i.e. 300/3000, 450/4500 and 600/6000 (mm/min)/rpm), R_a and R_z increased for all types of cutting tool coatings. For example, when drilling using TiAlN coated tools at n = 6000 rpm and f = 600 mm/min, R_a was 28% and 54% higher than when drilling at 450/4500 and 300/3000 (mm/min/rpm), respectively. Similar trends were also observed for the other two coatings with an increase in the hole roughness ranging from 1% to 13%. This indicates that reducing the drilling time would be at the expense of an increased roughness [3].

In summary, the analysis of hole roughness metrics R_a and R_z in terms of cutting parameters leads to the conclusion that lower feed rates and spindle speeds produce a lower hole roughness regardless of the cutting tool coating used. In addition, the dry drilling of GLARE® laminates with different cutting tool coatings and within the experimental window adopted in this study, led to a range of surface roughness values for R_a between 1.1 and 2 μm. Previous literature and technical documents do not specify the acceptable surface roughness for GLARE® or fibre metal laminates recommended by the aerospace industry for the machining/drilling process. However, technical reports such as those published by Sandvik [55] reported common hole

surface roughness R_a requirements by the aerospace industry when drilling composite metal stacks to be less than 3.2 μm in composite layers/parts and less than 1.6 μm in aluminium or titanium layers/parts [3]. Comparing the roughness results obtained in this study with those from the literature discussed earlier, it can be said that the R_a data reported here are within the limits of recommended values and similar to those presented in previous studies on machining similar GLARE® grade and thickness under dry conditions [2, 3]. It is also interesting to note that the TiAlN coating was shown in former investigations to yield better performance and improved surface roughness when machining aluminium alloys and composites in dry machining applications when compared to other coatings, even including TiN [2, 54, 56]. However, this was not the case in the current study. This could indicate that the interaction of alternating metal-composite layers in GLARE® laminates with the cutting tool has a significant impact on hole surface finish. It can be speculated that the TiAlN coating is less suitable for machining hybrid composite-metal materials such as GLARE® than TiN coating when the composite is made of glass fibre.

3.2 Burr formation analysis

Several burr caps were formed in each hole as shown in Fig.8, which tended to separate when the cutting tool cut through the last aluminium sheet in the workpiece [3, 18, 20]. The deformed aluminium sheets near the edge of the hole are continuously stretched and thinned causing them to fracture and form small uniform discontinuous burrs around the hole edge [3, 57]. The locations were burr caps separated from the workpiece showed significant burr formation compared to other regions around the hole. Fig.9 and Fig.10 show the average burr height and burr root thickness at the entrance and exit side of the holes for different tool coatings and cutting parameters. Burrs were produced in all holes starting with the first one, indicating that it is not caused by tool wear. Generally, burr was produced on both entry and exit sides of each hole. The exit burr height and root thickness were considerably larger than for entrance burrs,

which agrees with previous studies [3, 18, 20]. This is mainly because burr formed at the entrance results from a tearing process which involves a bending action followed by clean shearing or lateral extrusion [3, 58], while exit burr is formed due to plastic deformation of the workpiece material in front of the chisel edge without cutting the material [3, 59].

Burr height at the entrance ranged between 4 µm and 20 µm while burr height at exit ranged between 22 µm and 76 µm. Similar results were previously reported when drilling the same GLARE® grade with TiAlN coated cutting tools [3]. A larger helix angle and increasing point angle tend to reduce burr height and thickness [35, 60]. The smallest and largest burr heights at the entrance occurred using TiN coated tools when drilling at $n = 3000$ rpm, $f = 600$ mm/min and $n = 3000$ rpm, $f = 300$ mm/min, respectively. The largest burr height at the exit occurred when drilling at $n = 4500$ rpm, $f = 300$ mm/min using TiAlN coated tools, while the smallest burr height at the exit occurred at $n = 4500$ rpm, $f = 300$ mm/min using TiN coated tools. Burr height at exit was largest when using TiAlN coated tools, while AlTiN/TiAlN coated tools produced higher exit burrs than TiN coated tools when drilling at spindle speeds of $n = 3000$. TiN coated tools produced greater burr height at exit compared to AlTiN/TiAlN coated tools when drilling at higher spindle speeds of $n = 4500$ and 6000 rpm.

Based on the ANOVA study reported in Table 5, it can be observed that the feed rate was the primary contributing parameter on entry burr height with 22.61%, followed by minor contributions from the spindle speed with 5.57% and the cutting tool coating with 3.47%. For the exit burr height, the cutting tool coating was the primary contributing parameter with 71.47% followed by minor contributions from the spindle speed with 5.93% and the feed rate with 2.69%. These results indicate that burr height is a function of both the feed rate and the cutting tool coating. The linear interactions between the feed rate, spindle speed and tool coating had a significant contribution on entry burr height. For example, the interactions of the spindle speed with the feed rate and the spindle speed with the cutting tool coating were 25.13%

and 12.87%, respectively, while the interaction of the feed rate with the cutting tool coating was 13.3%. The linear interaction between the input parameters was less significant at exit burr height and did not exceed 10%.

As shown in Fig.10, for AlTiN/TiAlN and TiN coatings, burr root thickness at both sides tended to increase with the increase of the feed rate under all spindle speeds. For TiAlN coating, the burr root thickness at both sides tended to increase with the increase of the feed rate when drilling at $n = 3000$ and 6000 rpm. Burr root thickness at entrance ranged between 0.08 mm and 0.15 mm, while burr root thickness at exit ranged between 0.09 mm and 0.181 mm. Again, similar results were reported when drilling the same GLARE® grade and TiAlN coated cutting tools [3]. The largest burr root thickness at entrance resulted from drilling at $n = 4500$ rpm, $f = 450$ mm/min using TiAlN cutting tool, while the smallest burr root thickness at entrance occurred at $n = 6000$ rpm, $f = 450$ mm/min using TiN coated tools. The largest burr root thickness at exit resulted from drilling at $n = 3000$ rpm, $f = 450$ mm/min using TiAlN coated tools, while the smallest burr root thickness at exit occurred at $f = 300$ mm/min and spindle speeds of $n = 4500$ and 6000 rpm using TiN and AlTiN/TiAlN coated tools, respectively. Generally, TiN coated tools produced smaller burr root thickness at the entrance when drilling at a higher spindle speeds of $n =$ 4500, and 6000 rpm compared to the other two coatings, while TiAlN coated tools tended to produce largest burr root thickness at the exit amongst the other two coatings. The TiN and AlTiN/TiAlN coated tools produced relatively similar burr root thicknesses at the exit.

From the ANOVA results given in Table 5, the cutting tool coating was identified as the primary contributing parameter on entry burr root thickness with 19.28%, followed by less significant contributions from the feed rate with 12.39% and the spindle speed with 4.21%. For the exit burr root thickness, again the cutting tool coating had the largest contribution 62.32% followed by minor contributions from the feed rate with 15.03% and the spindle speed 4.59%.

These results indicate that burr root thickness is a function of the cutting tool coating. These observation are in-line with results reported when machining Al2024-T351 and Al6061-T6 alloys using TiAlN and TiCN coatings [61]. The linear interactions between the spindle speed and the other two parameters had a significant contribution on entry root thickness with up to 26.02% in three-way interactions, the interaction of spindle speed with the feed rate and the cutting tool coating had the most significant contribution. However, the percentage contribution of their interactions was less significant at exit burr root thickness and did not exceed 5%. Drilling at spindle speed/feed rate rations of 0.1 showed that burr height at entrance and exit increased with the increase of the feed rate and spindle speed. Similarly, with the observation made when analysing the surface roughness, this indicates that drilling at faster rates would be at the expense of reduced hole quality. Previous studies showed that TiAlN coated tools had a better wear resistance than those with TiN coating. Nevertheless, in the specific context of machining GLARE®, it is interesting to find that TiN coated tools produced smaller burrs than TiAlN coated ones and a slightly better surface finish [62, 63]. Reported literature indicated that good hole quality was achieved when using TiAlN coating when drilling aluminium alloys, including the Al2024 alloy [2, 27, 64]. A similar conclusion can be made on hole quality achieved in GLARE® laminates from the current study, but this can be also extended to include TiN and AlTiN/TiAlN coatings. TiAlN and AlTiN/TiAlN coatings are designed for machining materials with highly abrasive contents and dry drilling applications [8], such as the S2-glass fibre layers in GLARE®.

3.3 Cutting tool inspection

The cutting tools were inspected post machining process using a Dino-Lite portable USB optical microscope. The images were processed using the DinoCapture 2.0 software. Limited tool wear was observed on the cutting tools, as shown in Fig.11. No adhesion of aluminium chips was observed on the primary and secondary facets of all the cutting tools. Minor built up

edge was observed on the cutting lips of the TiN and AlTiN/TiAlN coated tools, while none were found on those with TiAlN coating. The BUE formed on TiN coated tools was relatively more than that found on AlTiN/TiAlN tools. This is mainly due to the higher thermal stability of AlTiN/TiAlN coatings at the tool tip for temperatures encountered in the drilling process. This higher thermal stability is due to the tendency of the TiAlN coatings to form a protective outermost layer of Al_2O_3 and an intermediate layer consisting from titanium, aluminium, oxygen, and nitrogen during the machining operation leading to higher oxidation resistance [2, 65, 66].

The chisel edge is not cutting but rather pushing through the laminate which resulted in adhesion of aluminium on the flank near the chisel edge similar to previous studies on drilling GLARE® [13]. Minor adhesion and wear in the form of coating delamination concentrated at the chisel edge, below the chisel edge tip and on the rake faces of all cutting tools. The discontinuous chip formation when cutting through aluminium sheets in the laminate promoted the flaking of the coating at the rake face regions and upper section of the flutes [67]. In addition, the abrasive nature of glass fibres caused minor wear at the outer corners of the drills as shown in Fig.11.

Minor chipping was observed on one of the cutting lips of the TiN coated tool possibly caused by thermal cracking due to high feed rates and spindle speeds. When the built-up is dislodged, it pulls away part of the coating and increases the likelihood of chipping the cutting edge as shown in Fig.12. No chipping was observed in the TiAlN and AlTiN/TiAlN coated tools due to their higher hardness compared to TiN-coated tools and due to the fact that there is less BUE for such tools. Similar tool wear mechanisms were observed when machining medium carbon alloy steel using TiN and TiAlN coatings [68]. It can be also speculated that chipping of main cutting edges in TiN coated tool is associated with edge or coating defects or simply due to accidents when handling the drill bits as shown in Fig.13.

Overall, visual and microscopic inspection of all cutting tools did not show any signs of severe wear after drilling each set of nine holes under different spindle speeds and feed rates. However, it can be concluded that although the coating used on drills can significantly improve the status of the surface, it does not prevent the phenomenon of adhesion of aluminium on the cutting edges and loss of coating [69]. It can be concluded that TiN coating has a higher erosion rate than TiAlN and AlTiN coatings, which agrees with previously reported studies [70, 71]. The microscopic images and SEM analysis of cutting tools after machining shows small presence of aluminium adhering on the cutting edges (BUE) in TiN and AlTiN/TiAlN coated tools and none in TiAlN coated tools, chisel edge and outer corners of the tools. Wear debris and transferred chip fragments during the drilling process were observed to adhere on the primary and secondary facets of the drill bits. The debris are continuously smeared and sheared on the cutting tool facets covering the worn surfaces as shown in Fig.14 and Fig.15.

At the same time, it was observed earlier that TiN coating exhibits a better tribological behaviour compared to the TiAlN coated tools in terms of burr formation and surface roughness. This is in line with the report made in [72]. However, this is only true when drilling a few holes using the same tool. The impact of drilling more holes using a single tool might be different and will be the purpose of a future study. Therefore, when considering tool-life as an additional machining dimension, the TiAlN coated tools should be more suitable for large-scale drilling applications of hybrid aerospace materials, such as GLARE®. The addition of aluminium to titanium nitride coating enhances the hardness of the tool and the natural formation of a thin aluminium oxide layer on its surface at elevated temperatures results in improved anti-oxidation property making TiAlN coatings suitable for dry and high-speed cutting [73].

3.4 Qualitative hole inspection under optical microscopy

Visually inspecting the hole and using an optical microscope, it was observed that the damage was smaller around the hole edges at the entrance than at the exit side. In addition, the hole edge quality at both sides decreased with the increase of the feed rate and spindle speed. The best visual hole quality was achieved at $n = 6000$ rpm and $f = 300$ mm/min and at $n = 3000$ rpm and $f = 300$ mm/min for TiN coated tools at top and bottom respectively while this was at $n = 3000$ rpm and $f = 300$ mm/min for both TiAlN and AlTiN/TiAlN coated tools at top and bottom, respectively. Using those cutting parameters, the hole edge was uniform with little or no visible burrs or deformations compared to the other holes. Images of hole surface at entry and exit sides for different cutting parameters and one set for each of the cutting tool coatings is provided in the supplementary material.

4. Conclusions

In this study, the machinability of GLARE® laminate was investigated through twist drilling operations to evaluate hole quality in terms of surface roughness and burr formation metrics. More specifically, these included R_a (average surface roughness) and R_z (ten-point mean roughness) as well as the burr height and the burr root thickness. The specific aim was to evaluate the impact of cutting parameters (spindle speed and feed rate) and particularly, of cutting tool coatings, namely TiAlN, TiN and AlTiN/TiAlN coatings on the achieved hole quality in GLARE® 2B fibre metal laminates. This study was motivated by the fact that the effect of cutting tool coatings on the hole quality had been previously tested on different GLARE® grades but never in a single study using a fixed tool geometry. The influence of tool coatings is an important issue in machining hybrid aerospace materials and at the same time, limited research has been carried out on the machinability of GLARE® laminates in general. The following results can be concluded from the reported study:

- The highest R_a and R_z values were found when drilling with TiAlN coated tools and lowest when using TiN coated tools. R_a and R_z increased with the increase of spindle speed regardless of cutting tool used, while the influence of the feed rate varied depending on the type of the cutting tool coating. The analysis of hole roughness parameters leads to the conclusion that using lower feed rates and spindle speeds produces better hole roughness regardless of the cutting tool coating utilised.
- Burrs were produced on entry and exit sides of the hole; the exit burr height and burr root thickness were considerably larger than entrance burrs. The feed rate was the primary contributing parameter on entry burr height, the tool coating was the primary contributing parameter on exit burr height, while the cutting tool coating was also the primary contributing parameter on entry burr root thickness and exit burr root thickness.
- TiN coated tools showed a higher erosion rate than TiAlN and AlTiN coatings, while it also exhibited a better tribological behaviour overall in terms of burr formation and surface roughness
- Machining debris and transferred chip fragments during the drilling process were observed to adhere on the primary and secondary facets of the drill bits. The wear mechanism observed on the drill flank, drill bit faces, cutting lips and chisel edge of the drills was found to be a mixture of abrasion, coating delamination and minor built-up edge.

Acknowledgements

The authors would like to thank the Dr. Peter J. Kortbeek from DELFT University and the Fibre-Metal Laminate Centre of Competence (FMLC) for the provision of GLARE® sample. The authors acknowledge the support from the European Regional Development Fund through the Welsh Government for ASTUTE 2020 (Advanced Sustainable Manufacturing Technologies) to facilitate this work.

Data availability

The raw data required to reproduce these findings are available upon request.

References

1. Vlot, A. and J.W. Gunnink, *Fibre metal laminates: an introduction*. 2001: Springer.
2. Giasin, K., S. Ayvar-Soberanis, and A. Hodzic, *An experimental study on drilling of unidirectional GLARE fibre metal laminates.* Composite Structures, 2015. **133**: p. 794-808.
3. Giasin, K., *Machining Fibre Metal Laminates and Al2024-T3 aluminium alloy*. 2017, University of Sheffield.
4. Pora, J., *Composite materials in the airbus A380–from history to future.* Proceedings of ICCM13, Plenary lecture, CD-ROM, 2001.
5. Graham-Cumming, J., *The Geek Atlas: 128 places where science and technology come alive*. 2009: " O'Reilly Media, Inc.".
6. Quilter, A., *Composites in aerospace applications.* IHS White Paper, 2001. **444**(1).
7. Sinke, J., *Manufacturing of GLARE parts and structures.* Applied composite materials, 2003. **10**(4-5): p. 293-305.
8. Kalidas, S., R.E. DeVor, and S.G. Kapoor, *Experimental investigation of the effect of drill coatings on hole quality under dry and wet drilling conditions.* Surface and Coatings Technology, 2001. **148**(2): p. 117-128.
9. Hogan, B.J., *Automation Speeds A380 Wing Assembly*, in *Manufacturing Engineering Magazine*

2005, sme.org: sme.org.
10. Hocheng, H., *Machining technology for composite materials : principles and practice*. 2012, Cambridge, UK; Philadelphia, PA: Woodhead Pub.
11. Krishnaraj, V., R. Zitoune, and J.P. Davim, *Drilling of polymer-matrix composites*. 2013: Springer.
12. Groover, M.P., *Fundamentals of modern manufacturing: materials processes, and systems*. 2007: Wiley. com.
13. J.F.W.Coesel, *Drilling Of Fibre-Metal Laminates*, in *Faculty of Aerospace Engineering*. 1994, Delft University of Technology. p. 63.
14. Tyczynski, P., J. Lemanczyk, and R. Ostrowski, *Drilling of CFRP, GFRP, glare type composites.* Aircraft Engineering and Aerospace Technology, 2014. **86**(4): p. 312-322.
15. Pawar, O.A., et al., *Analysis of hole quality in drilling GLARE fiber metal laminates.* Composite Structures, 2015. **123**: p. 350-365.
16. Giasin, K., S. Ayvar-Soberanis, and A. Hodzic, *The effects of minimum quantity lubrication and cryogenic liquid nitrogen cooling on drilled hole quality in GLARE fibre metal laminates.* Materials & Design, 2016. **89**: p. 996-1006.
17. Giasin, K. and S. Ayvar-Soberanis, *Evaluation of Workpiece Temperature during Drilling of GLARE Fiber Metal Laminates Using Infrared Techniques: Effect of Cutting Parameters, Fiber Orientation and Spray Mist Application.* Materials, 2016. **9**(8): p. 622.
18. Giasin, K., S. Ayvar-Soberanis, and A. Hodzic, *Evaluation of cryogenic cooling and minimum quantity lubrication effects on machining GLARE laminates using design of experiments.* Journal of Cleaner Production, 2016. **135**: p. 533-548.
19. Giasin, K., et al., *3D Finite Element Modelling of Cutting Forces in Drilling Fibre Metal Laminates and Experimental Hole Quality Analysis.* Applied Composite Materials, 2016: p. 1-25.
20. Giasin, K. and S. Ayvar-Soberanis, *An Investigation of burrs, chip formation, hole size, circularity and delamination during drilling operation of GLARE using ANOVA.* Composite Structures, 2017. **159**: p. 745-760.
21. Giasin, K. and S. Ayvar-Soberanis, *Microstructural investigation of drilling induced damage in fibre metal laminates constituents.* Composites Part A: Applied Science and Manufacturing, 2017. **97**: p. 166-178.
22. Park, S.Y., et al., *Effect of drilling parameters on hole quality and delamination of hybrid GLARE laminate.* Composite Structures, 2017.
23. Giasin, K., *The effect of drilling parameters, cooling technology, and fiber orientation on hole perpendicularity error in fiber metal laminates.* The International Journal of Advanced Manufacturing Technology, 2018.
24. Haan, D., et al., *An experimental study of cutting fluid effects in drilling.* Journal of Materials Processing Technology, 1997. **71**(2): p. 305-313.

25. Braga, D.U., et al., *Using a minimum quantity of lubricant (MQL) and a diamond coated tool in the drilling of aluminum–silicon alloys.* Journal of Materials Processing Technology, 2002. **122**(1): p. 127-138.
26. Nouari, M., et al., *Effect of machining parameters and coating on wear mechanisms in dry drilling of aluminium alloys.* International Journal of Machine Tools and Manufacture, 2005. **45**(12–13): p. 1436-1442.
27. Kurt, M., Y. Kaynak, and E. Bagci, *Evaluation of drilled hole quality in Al 2024 alloy.* The International Journal of Advanced Manufacturing Technology, 2008. **37**(11): p. 1051-1060.
28. Ashrafi, S.A., et al., *Performance evaluation of carbide tools in drilling CFRP-Al stacks.* Journal of composite materials, 2013.
29. Alderliesten, R.C., *Fatigue crack propagation and delamination growth in Glare*. 2005: DUP Science.
30. Youssef, H.A. and H. El-Hofy, *Machining technology: machine tools and operations*. 2008: CRC Press.
31. Davim, J.P., *Modern machining technology: A practical guide*. 2011: Elsevier.
32. Giasin, K., et al., *Assessment of cutting forces and hole quality in drilling Al2024 aluminium alloy: experimental and finite element study.* The International Journal of Advanced Manufacturing Technology, 2016. **87**(5-8): p. 2041-2061.
33. Joseph, R. and J. Davis, *Aluminium and Aluminium Alloys.* ASM International, Materials Park, OH, 1993.
34. Nouari, M., et al., *Experimental analysis and optimisation of tool wear in dry machining of aluminium alloys.* Wear, 2003. **255**(7): p. 1359-1368.
35. Ko, S.-L. and J.-K. Lee, *Analysis of burr formation in drilling with a new-concept drill.* Journal of Materials Processing Technology, 2001. **113**(1–3): p. 392-398.
36. Stephenson, D.A. and J.S. Agapiou, *Metal cutting theory and practice*. 2016: CRC press.
37. Heinemann, R., et al., *Effect of MQL on the tool life of small twist drills in deep-hole drilling.* International Journal of Machine Tools and Manufacture, 2006. **46**(1): p. 1-6.
38. Chim, Y., et al., *Oxidation resistance of TiN, CrN, TiAlN and CrAlN coatings deposited by lateral rotating cathode arc.* Thin Solid Films, 2009. **517**(17): p. 4845-4849.
39. Minitab, *Understanding Analysis of Variance (ANOVA) and the F-test*, in *Understanding Analysis of Variance (ANOVA) and the F-test*, M.B. Editor, Editor. 2016, Minitab.
40. Giasin, K., et al., *Assessment of cutting forces and hole quality in drilling Al2024 aluminium alloy: experimental and finite element study.* The International Journal of Advanced Manufacturing Technology, 2016: p. 1-21.
41. Zitoune, R., V. Krishnaraj, and F. Collombet, *Study of drilling of composite material and aluminium stack.* Composite Structures, 2010. **92**(5): p. 1246-1255.
42. Phadnis, V.A., et al., *Drilling in carbon/epoxy composites: Experimental investigations and finite element implementation.* Composites Part A: Applied Science and Manufacturing, 2013. **47**: p. 41-51.
43. Blau, P., R. Martin, and L. Riester, *A comparison of several surface finish measurement methods as applied to ground ceramic and metal surfaces*. 1996, Oak Ridge National Lab., TN (United States).
44. König, W. and P. Grass, *Quality definition and assessment in drilling of fibre reinforced thermosets.* CIRP Annals-Manufacturing Technology, 1989. **38**(1): p. 119-124.
45. Gillespie, L.K., *Deburring precision miniature parts.* Precision Engineering, 1979. **1**(4): p. 189-198.
46. Choi, I.H. and J.D. Kim, *Electrochemical deburring system using electroplated CBN wheels.* International Journal of Machine Tools and Manufacture, 1998. **38**(1): p. 29-40.
47. PILNÝ, B.L., *High speed drilling of aluminium plates*, in *Faculty of Mechanical engineering- Institute of manufacturing technology*. 2011, BRNO Univresity of technology. p. 151.
48. Mann, J.Y. and I.S. Milligan, *Aircraft Fatigue: Design, Operational and Economic Aspects*. 2013: Elsevier Science.
49. Dornfeld, D., *Strategies for preventing and minimizing burr formation.* 2004.
50. Biermann, D. and M. Heilmann, *Burr minimization strategies in machining operations*, in *Burrs-Analysis, Control and Removal*. 2010, Springer. p. 13-20.
51. Schäfer, F., et al., *Entgraten: Theorie, Verfahren, Anlagen*. 1975: Krausskopf.
52. Pramanik, A. and G. Littlefair, *Developments in Machining of Stacked Materials Made of CFRP and Titanium/Aluminum Alloys.* Machining Science and Technology, 2014. **18**(4): p. 485-508.
53. Liew, W.Y., et al., *Frictional and wear behaviour of AlCrN, TiN, TiAlN single-layer coatings, and TiAlN/AlCrN, AlN/TiN nano-multilayer coatings in dry sliding.* Procedia Engineering, 2013. **68**: p. 512-517.
54. Shunmugesh, K. and P. Kavan, *Investigation and optimization of machining parameters in drilling of carbon fiber reinforced polymer (CFRP) composites.* PIGMENT & RESIN TECHNOLOGY, 2017. **46**(1): p. 21-30.

55. coromant, S., *Machining carbon fibre materials*, in *Sandvik coromant user's guide - composite solutions* 2010.
56. Shareef, I., M. Natarajan, and O.O. Ajayi. *Dry machinability of aluminum alloys*. in *World Tribology Congress III*. 2005. American Society of Mechanical Engineers.
57. Stringer, P., G. Byrne, and E. Ahearne, *Tool design for burr removal in drilling operations*.
58. Hashmi, S., *Comprehensive Materials Processing*. 2014: Newnes.
59. Min, S. and D. Dornfeld, *Technology assessment on current advanced research projects in burr formation and deburring.* Report, The Association for Manufacturing Technology, 2004.
60. Dornfeld, D., et al., *Drilling burr formation in titanium alloy, Ti-6AI-4V.* CIRP Annals-Manufacturing Technology, 1999. **48**(1): p. 73-76.
61. Niknam, S.A. and V. Songmene, *Factors governing burr formation during high-speed slot milling of wrought aluminum alloys.* Proceedings of the Institution of Mechanical Engineers, Part B: Journal of Engineering Manufacture, 2013. **227**(8): p. 1165-1179.
62. Imbeni, V., et al., *Tribological behaviour of multi-layered PVD nitride coatings.* Wear, 2001. **251**(1-12): p. 997-1002.
63. Aramcharoen, A., et al., *Evaluation and selection of hard coatings for micro milling of hardened tool steel.* International Journal of Machine Tools and Manufacture, 2008. **48**(14): p. 1578-1584.
64. Kalidas, S., R.E. DeVor, and S.G. Kapoor, *Experimental investigation of the effect of drill coatings on hole quality under dry and wet drilling conditions.* Surface and Coatings Technology, 2001. **148**(2–3): p. 117-128.
65. Jindal, P., et al., *Performance of PVD TiN, TiCN, and TiAlN coated cemented carbide tools in turning.* International Journal of Refractory Metals and Hard Materials, 1999. **17**(1-3): p. 163-170.
66. Stephenson, D.A. and J.S. Agapiou, *Metal cutting theory and practice*. Vol. 68. 2005: CRC press.
67. Klocke, F., C. Nobel, and D. Veselovac, *Influence of Tool Coating, Tool Material, and Cutting Speed on the Machinability of Low-Leaded Brass Alloys in Turning.* Materials and Manufacturing Processes, 2016. **31**(14): p. 1895-1903.
68. Talib, R., H. Ariff, and M. Toff, *Wear mechanism of TiN, TiAIN and TiCN coated drills during drilling of carbon steel.* Journal of physical science, 2007. **18**(1): p. 75-85.
69. Zitoune, R., et al., *Influence of machining parameters and new nano-coated tool on drilling performance of CFRP/Aluminium sandwich.* Composites Part B: Engineering, 2012. **43**(3): p. 1480-1488.
70. Deng, J., et al., *Erosion wear of CrN, TiN, CrAlN, and TiAlN PVD nitride coatings.* International Journal of Refractory Metals and Hard Materials, 2012. **35**: p. 10-16.
71. Chauhan, K.V. and S.K. Rawal, *A review paper on tribological and mechanical properties of ternary nitride based coatings.* Procedia Technology, 2014. **14**: p. 430-437.
72. Rech, J., A. Kusiak, and J. Battaglia, *Tribological and thermal functions of cutting tool coatings.* Surface and Coatings Technology, 2004. **186**(3): p. 364-371.
73. Zhong, N., et al., *Microstructure and cutting performance of carbonitride coated tools in high speed machining of 40Cr steel.* Surface Engineering, 2011. **27**(4): p. 306-310.
74. Bi, S. and J. Liang, *Experimental studies and optimization of process parameters for burrs in dry drilling of stacked metal materials.* The International Journal of Advanced Manufacturing Technology, 2011. **53**(9): p. 867-876.
75. Beumler, T., *Flying GLARE: A Contribution to Aircraft Certification Issues in Strength Properties in Non-damaged and Fatigue Damaged GLARE Structures*. 2004: Delft University Press.
76. Kim, G.W. and K.Y. Lee, *Critical thrust force at propagation of delamination zone due to drilling of FRP/metallic strips.* Composite structures, 2005. **69**(2): p. 137-141.
77. Kim, D., M. Ramulu, and W. Pedersen, *Machinability of titanium/graphite hybrid composites in drilling.* Trans. NAMRI/SME, 2005. **33**: p. 445-452.
78. Kim, D. and M. Ramulu, *Study on the drilling of titanium/graphite hybrid composites.* Journal of Engineering Materials and Technology, 2007. **129**(3): p. 390-396.
79. Sánchez Carrilero, M., et al. *Dry drilling of fiber metal laminates CF/AA2024. A preliminary study*. in *Materials science forum*. 2006. Trans Tech Publ.
80. Pawar, O.A., et al., *Analysis of hole quality in drilling GLARE fiber metal laminates.* Composite Structures, 2015.
81. Senthilkumar, B.M.A., *Mechanical and Machinability Characteristics of Fiber Metal Laminates*. 2016: LAP Lambert Academic Publishing. 60.
82. Rezende, B.A., et al., *Investigation on the Effect of Drill Geometry and Pilot Holes on Thrust Force and Burr Height When Drilling an Aluminium/PE Sandwich Material.* Materials, 2016. **9**(9): p. 774.
83. Bañón, F., et al., *Preliminary study of the dry drilling process of CFRP/UNS A92024 stacks held together by adhesives.* Procedia Manufacturing, 2017. **13**(Supplement C): p. 211-218.

Figures

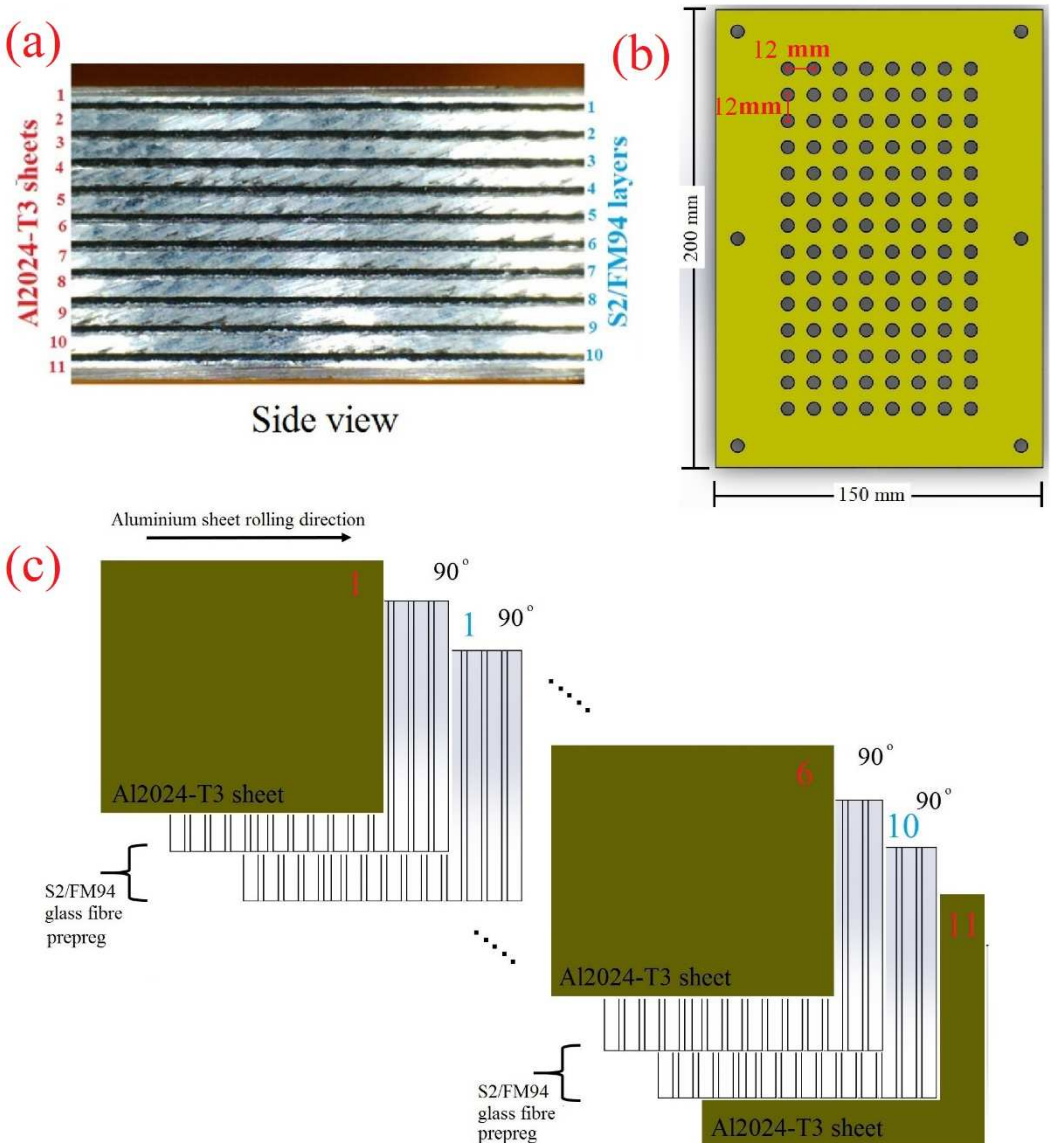

Fig.1: Details of the GLARE® 2B 11/10-0.4 specimen used for the drilling trials (a) Side view [3, 16] (b) Top view, also showing the location of holes to be drilled (c) detailed view showing fibre orientation and rolling direction

Fig. 2: Cutting tools used in the drilling trials

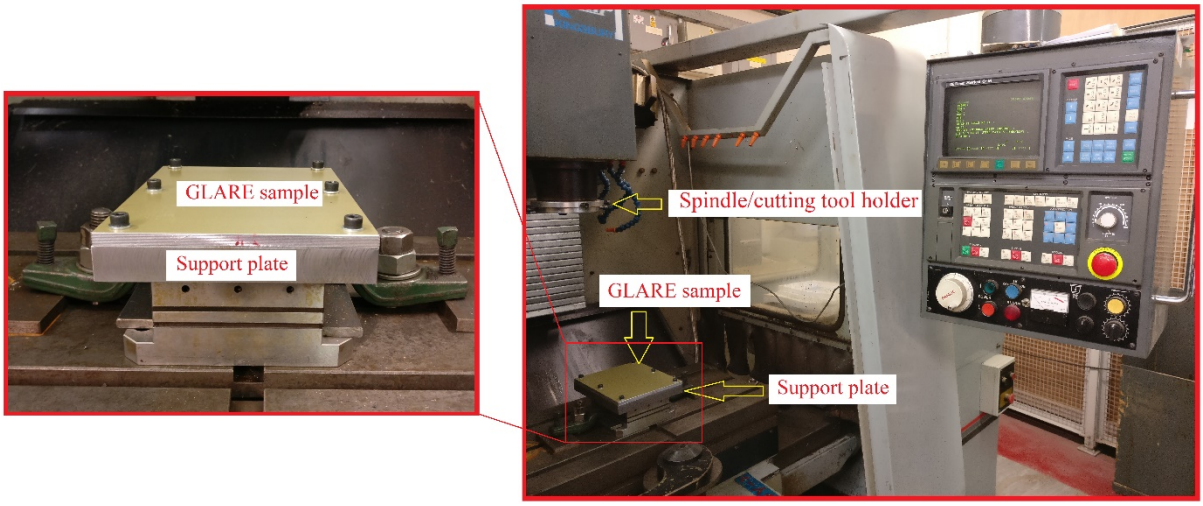

Fig.3: Details of the CNC machine and GLARE® 2B 11/10-0.4 specimen setup

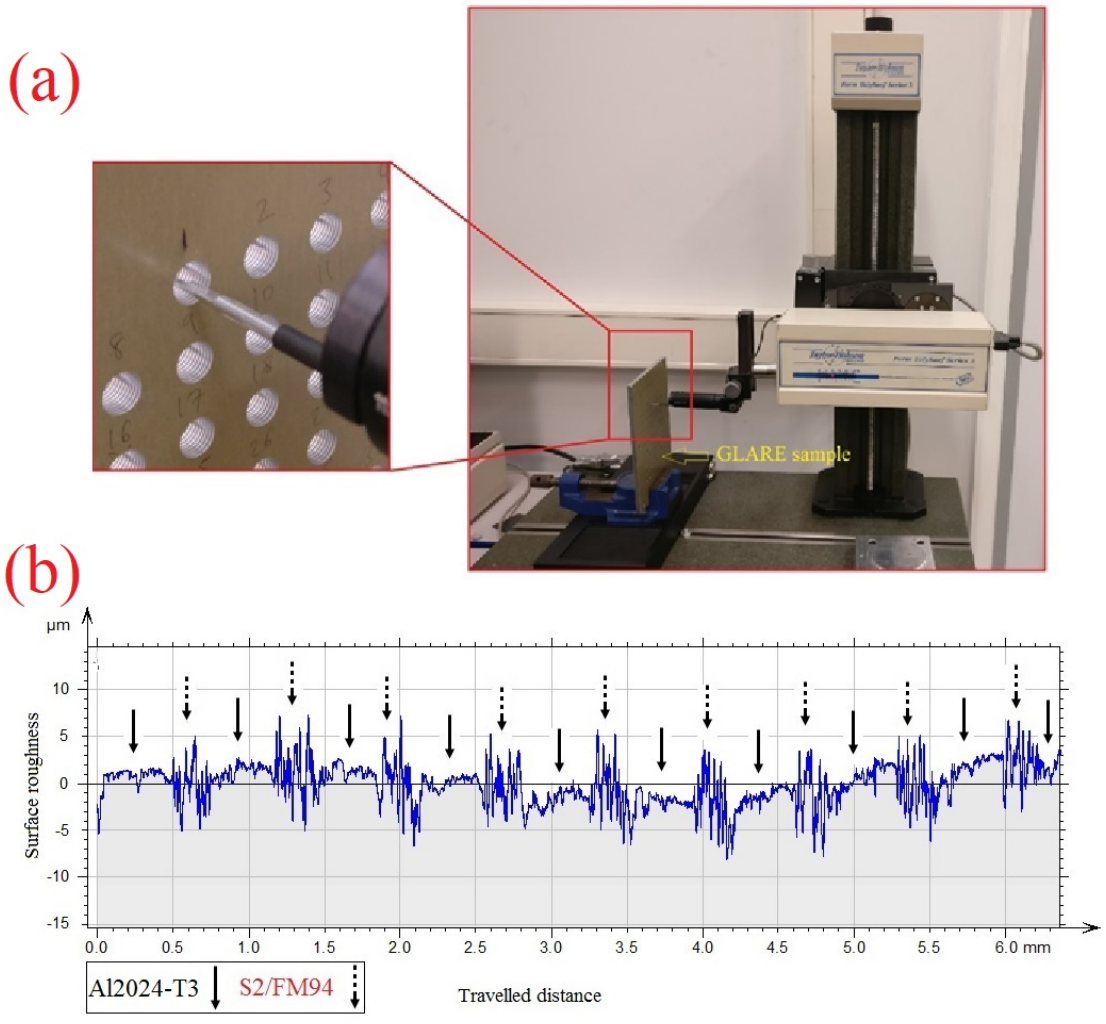

Fig.4: Details of measuring average roughness parameters of holes drilled in the GLARE® 2B 11/10-0.4 specimen showing (a) Measurement setup (b) Surface roughness profile

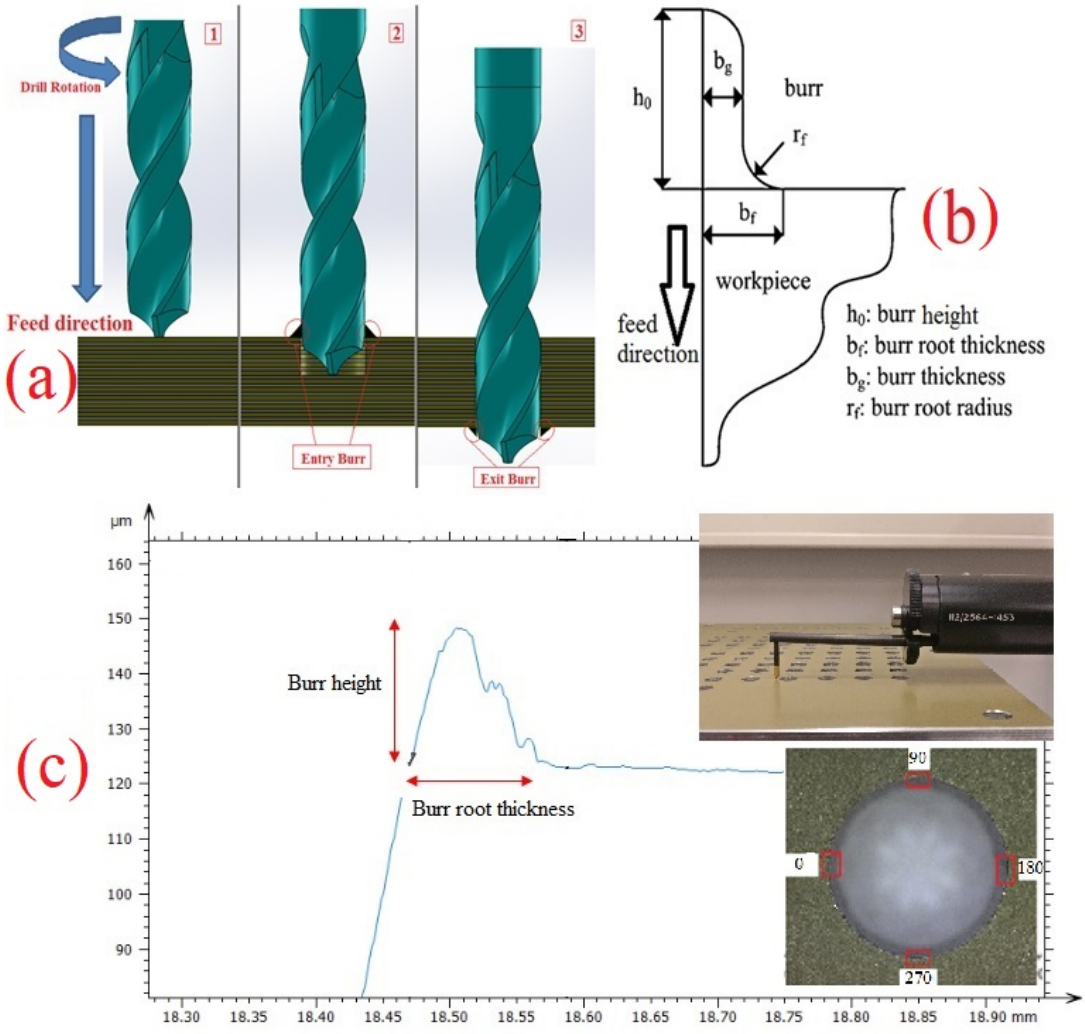

Fig.5: Burr profile showing a) the formation of burrs during drilling process [3, 74] b) a detailed description of burr parameters [3, 74] c) the measurement process and locations of burr height and burr root thickness

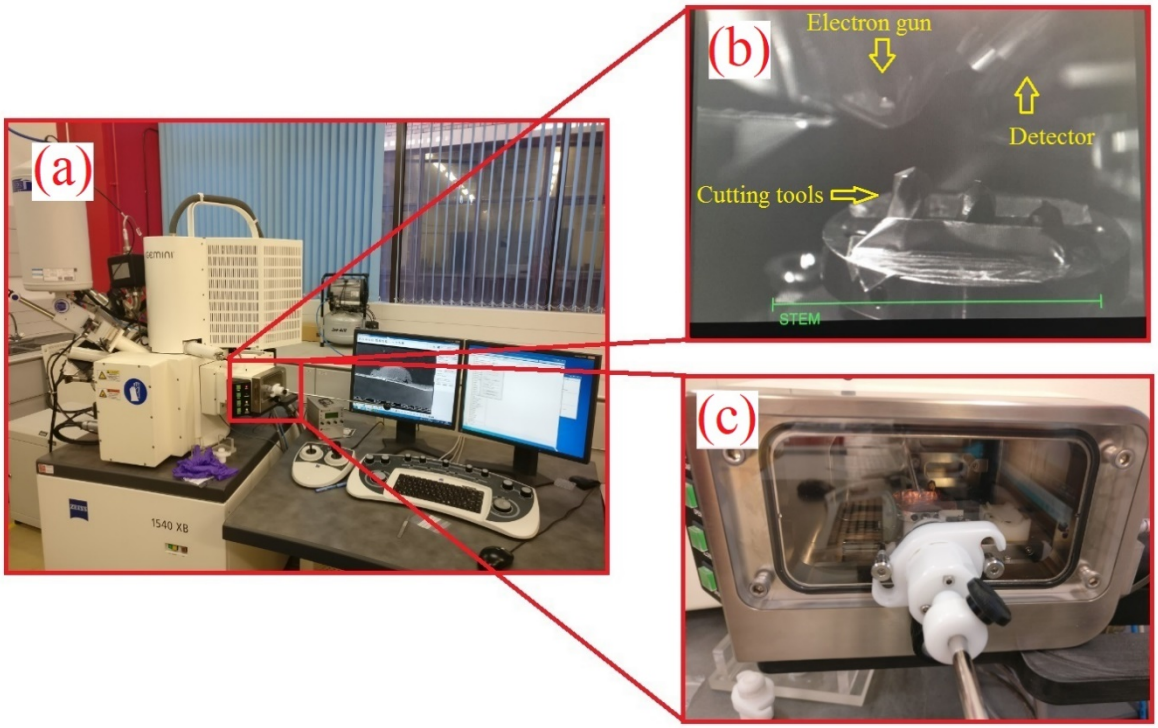

Fig.6: Photos showing (a) the Carl Zeiss 1540 XB SEM microscope (b) inside the main chamber with the cutting tools set up (c) the outer view of the SEM interlock

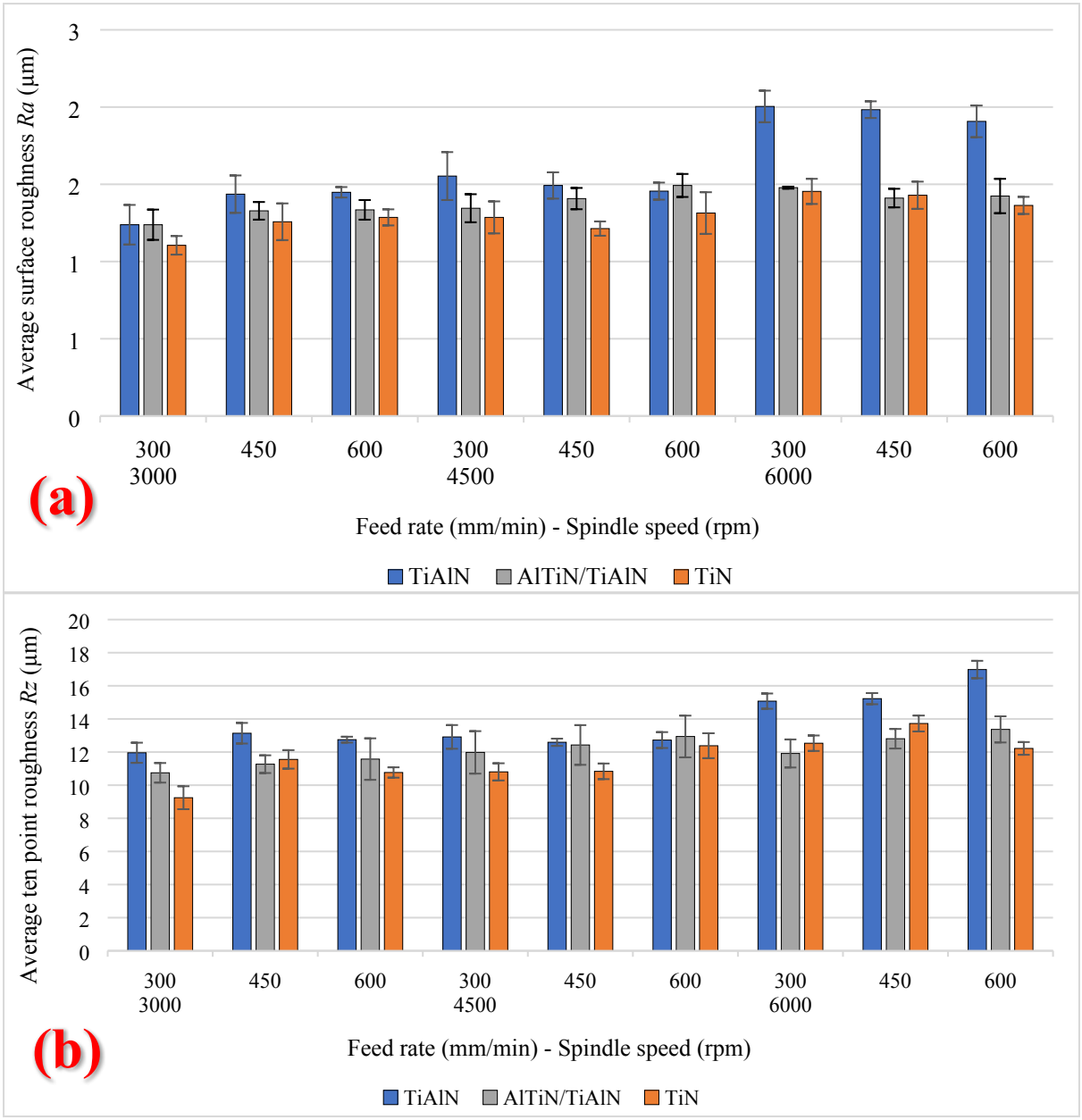

Fig.7: Average (a) arithmetic surface roughness R_a (b) ten-point mean roughness R_z

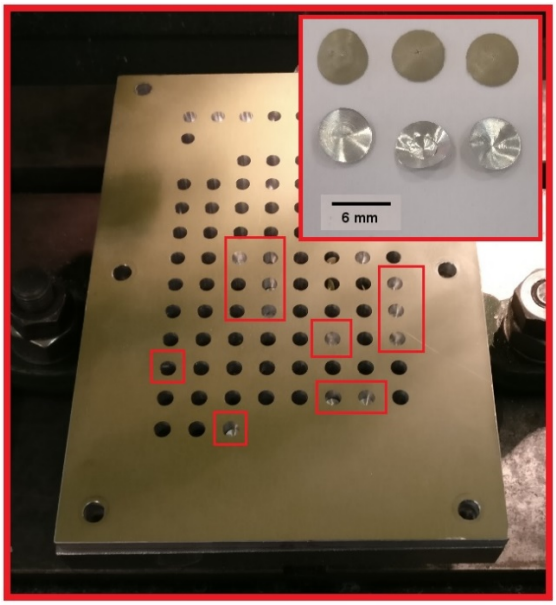

Fig.8: GLARE® workpiece showing formed burr caps after the drilling process

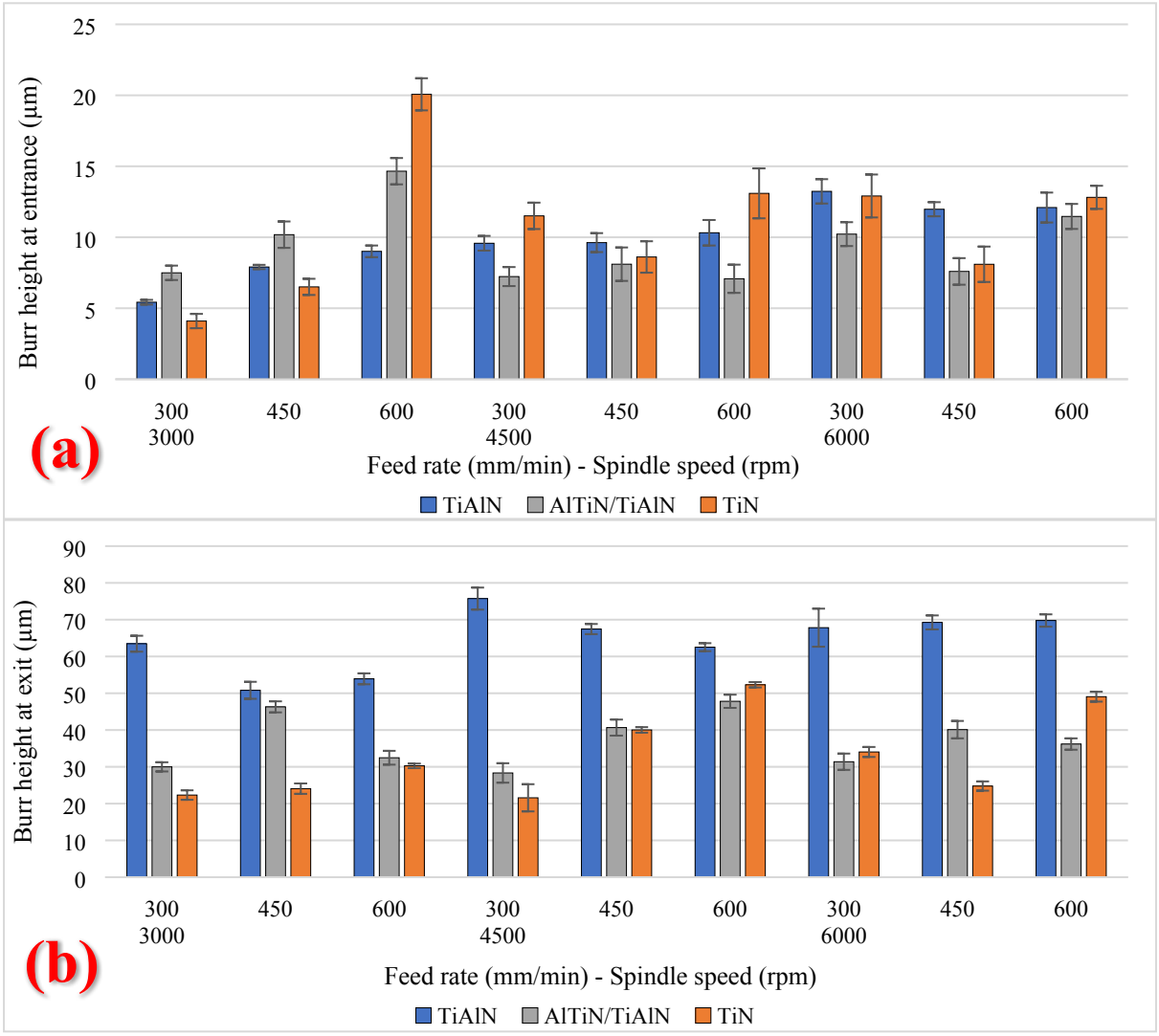

Fig.9: Average burr height at (a) entrance (b) exit

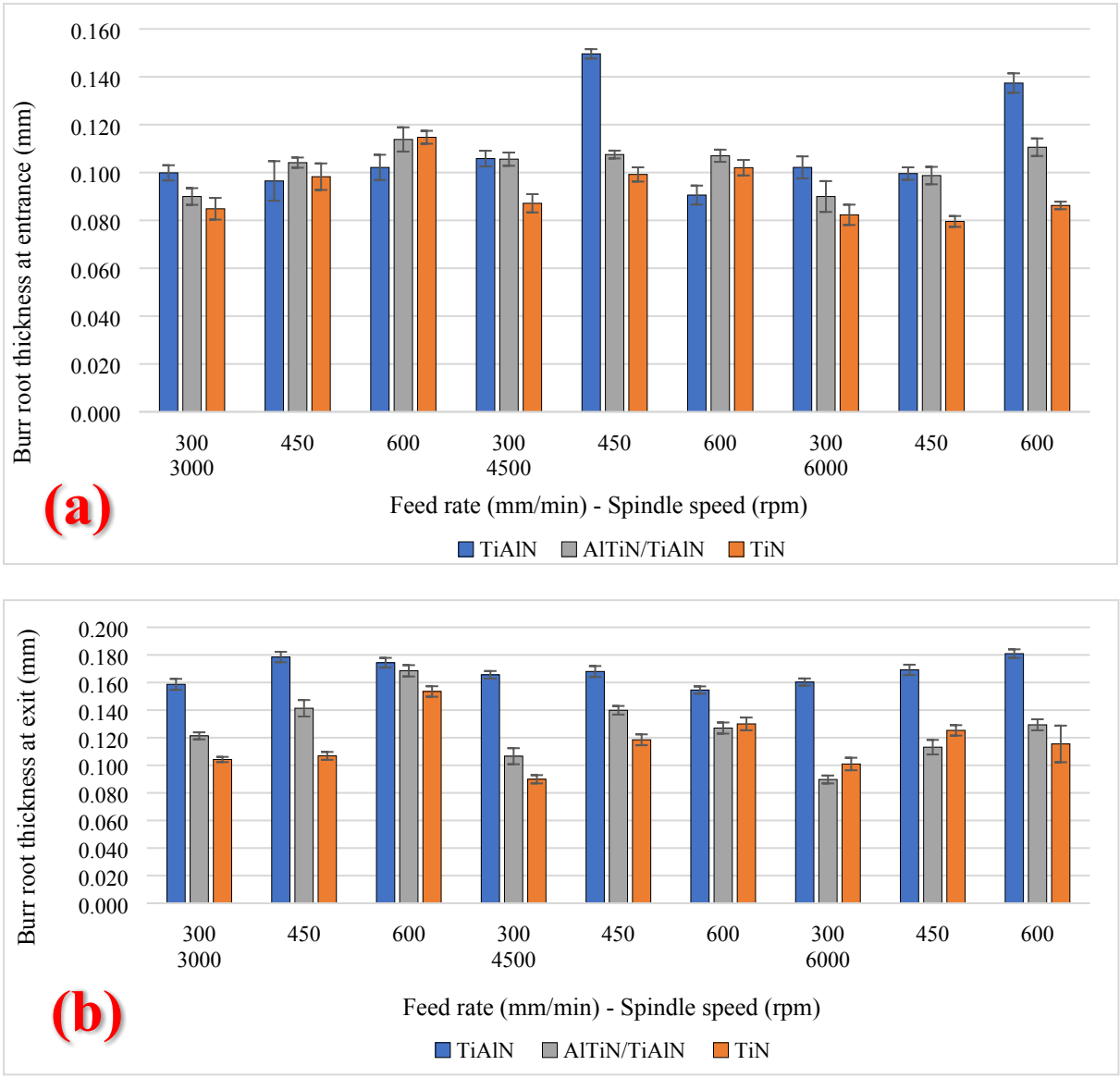

Fig.10: Average burr root thickness at (a) entrance (b) exit

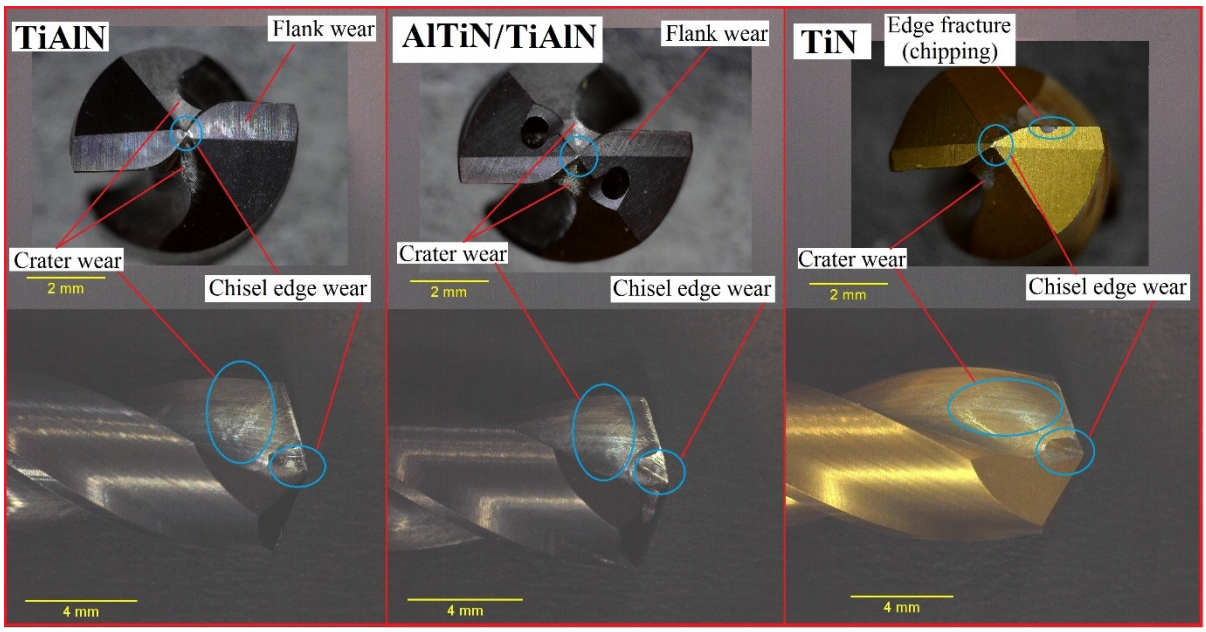

Fig.11: Post machining tool condition

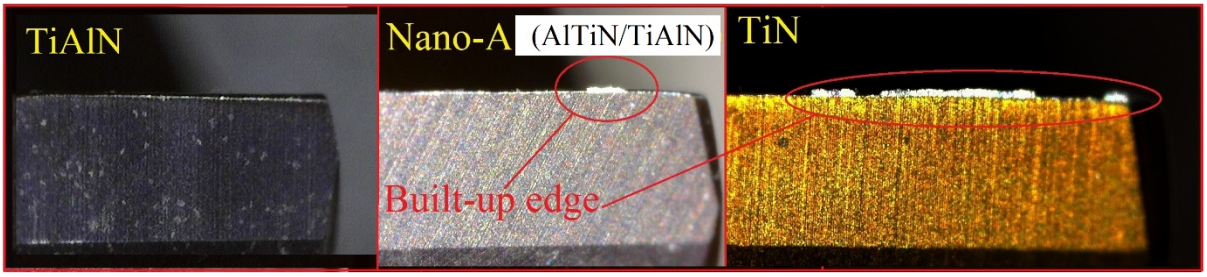

Fig.12: Microscopic images of cutting tool edges showing BUE in all three types of tools

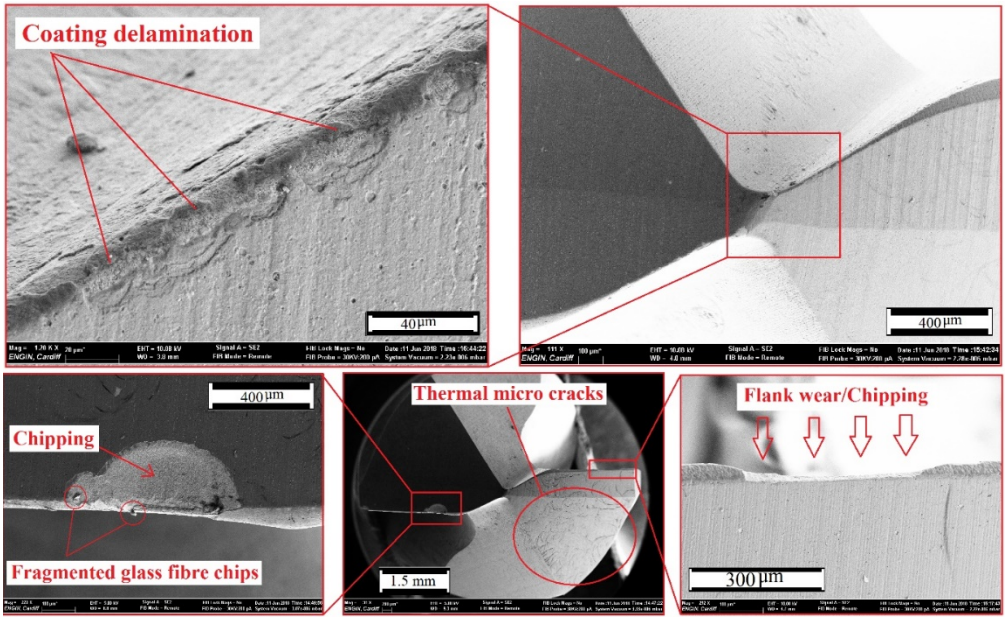

Fig.13: SEM images of TiN cutting tool post machining process

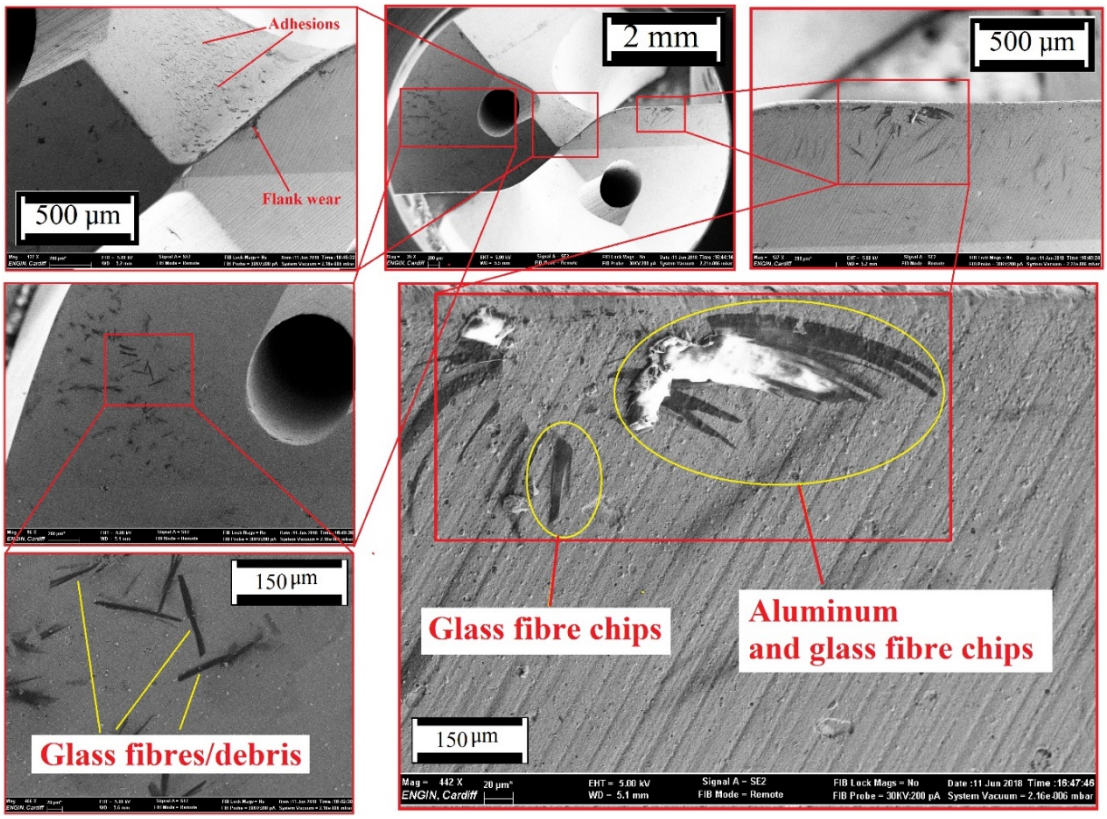

Fig.14: SEM images of AlTiN/TiAlN cutting tool post machining process

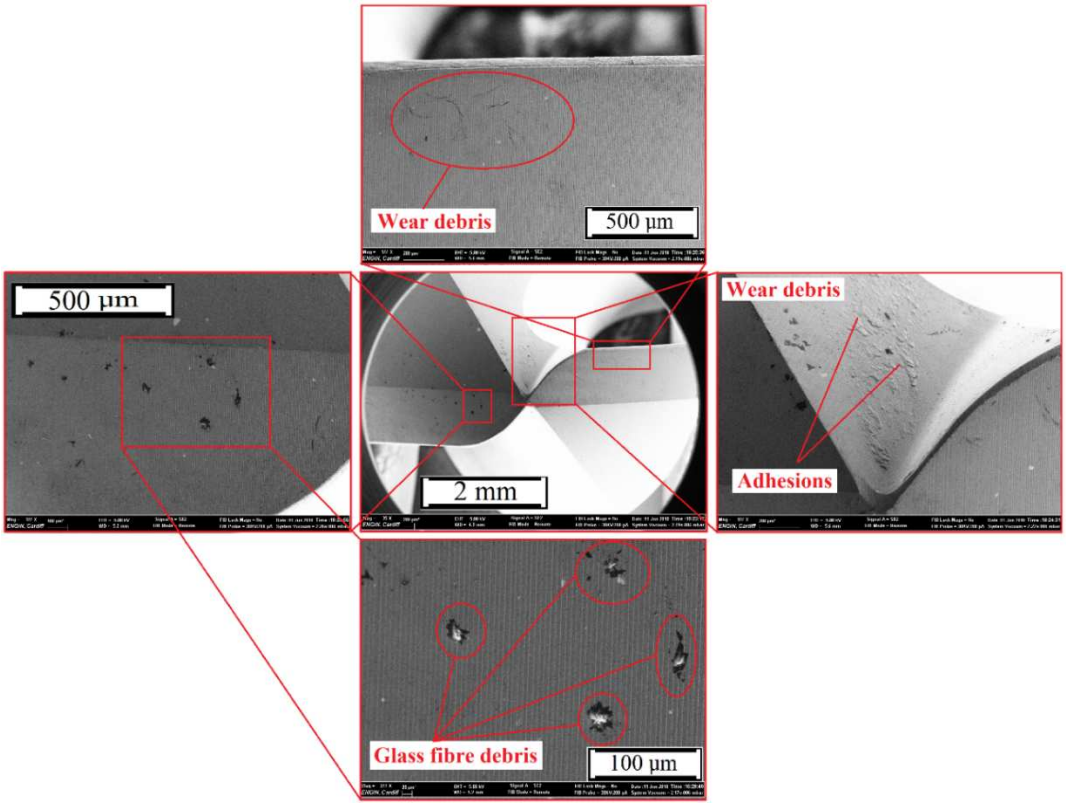

Fig.15: SEM images of TiAlN cutting tool post machining process

Tables

Table 1: Summary of previous studies on conventional and non-conventional drilling of fibre metal laminates [3, 21]

Material information	Cutting tool	Cutting parameters	Areas studied	Ref.
GLARE® 3-3/2-0.3 **GLARE® 3-2/1-0.3** **GLARE3®-4/3-0.3**	HSS TiN, HSS with 8% Co, Carbide tipped HSS, Solid carbide, Diamond tipped HSS 118°, 135° -point angle 4.8, 5- and 5.5-mm diameter	0.05, 0.08 and 0.13 (mm/rev) 40, 55, 70 and 140 (m/min)	CF, HC, HR, BF, CI	[13]
GLARE® 3	-	-	FC, SR, RIS	[75]
FRP/metallic strips	-	-	CF	[76]
Titanium/graphite hybrid composites (TiGr)	Carbide, Standard C2 grade solid carbide drill	1320, 2230, 3500, 5440 (rpm) 0.02, 0.03, 0.14, 0.25, and 0.3 (mm/rev)	CF, CE, HS, HR, BF, CHF	[77, 78]
CFRP/Al2024	TiN and CrN coated and non-coated WC-10Co drills	25-50 m/min 0.05 and 0.2 mm/rev	SR, TW	[79]
GLARE-like (Al2024/R-Glass)	6 mm diameter and 90°-point angle Uncoated VHM carbide drills	0.05, 0.075, 0.1, 0.125 and 0.15 (mm/rev) 75.36 (m/min) (4000 rpm)	SD, VI, CF, HS,	[14]
GLARE® 5 3/2-0.3 **GLARE® 6 3/2-0.3**	2,3,4 & 8 facets solid carbide drills with 120°-point angle, 30° helix angle and 6.35 mm diameter	0.15, 0.225 and 0.3 (mm/rev) 4500, 6000 and 7500 (rpm)	CF, HS, AE, CHF, D, BF, HS	[80]
GLARE® 2B 4/3-0.4 **GLARE® 2B 8/7-0.4** **GLARE® 2B 11/10-0.4** **GLARE® 3 8/7-0.4**	6 mm TiAlN coated solid carbide drills. 140°-point angle, 30° helix angle	100, 300, 600 and 900 (mm/min) 1000, 3000, 6000 and 9000 (rpm)	CF, SR, HS, HC, BF, DE, CHF, TW, P	[2, 16-21, 23]
GLARE® 2/1, GLARE® 3/2, GLARE® 5/4	4,6 and 8 mm HSS drills	-	D	[81]
Aluminium/ Polyethylene sandwich	2, 3- and 4-mm brad, spur, two flutes and three facet twist Tungsten Carbide drills	0.05, 0.1, 0.15 and 0.25 (m/rev) 24, 48, 72 (m/min)	CF, BF	[82]
CFRP/UNS A92024	-	200, 250 and 300 (mm/min) 85, 115 and 145	HS, SR, CHF	[83]
GLARE®3 4/3-0.4	HSS-cobalt solid cemented carbide K10 118°-point angle, 25° helix angle	0.04, 0.12 and 0.2 (mm/rev) 600, 1800 and 3000 (rpm)	CF, SR, D, BF, CHF, TW, HS, HC	[22]

AE: Absolute Energy, BF: Burr Formation, CE: Cutting Energy, CF: Cutting Forces, CHF: CHip Formation, CI: Crack Initiation, D: Delamination, FC: Fatigue Crack, HC: Hole Circularity, HR: Hole Roundness, HS: Hole Size, RIS: Rivet Strength, RS: Residual Strength, SD: Stress Distribution, SR: Surface Roughness, TW: Tool Wear, VI: Visual Inspection, P: Perpendicularity.

Table 2: Details of cutting tools and coatings used in the experiments

Description	**Tool A**	**Tool B**	**Tool C**
Tool material	Tungsten carbide		
Drill diameter (mm)	6		
Helix angle (°)	30		
Point angle (°)	140		
Tolerance	M7		
Coating	TiAlN	TiN	AlTiN/TiAlN
Colour	Violet black	Gold	Black
Coating thickness (µm)	1.5-4	1.5-4	1.5-5
Layer structure	mono layer	mono layer	multilayer
Nano hardness (HV 0.05)	3300	2400	3800
Friction coefficient	0.5-0.55	0.4-0.5	0.6
Thermal stability (°C)	700-800	595	900
Manufacturer	OSG®	GUHRING®	GUHRING®

Table 3: Details of cutting parameters used in the drilling experiments

Factor	**Level 1**	**Level 2**	**Level 3**
Spindle speed (rpm)	3000	4500	6000
Feed rate (mm/min)	300	450	600
Coating	TiAlN	TiN	AlTiN/TiAlN

Table 4: ANOVA table showing the percentage contribution of cutting parameters and cutting tool coating effect on surface roughness parameters

	Average surface roughness R_a						Ten-point mean roughness R_z					
Source	**DF**	**Adj SS**	**Adj MS**	**F-Value**	**P-Value**	**%**	**DF**	**Adj SS**	**Adj MS**	**F-Value**	**P-Value**	**%**
Model	28	3.91883	0.139958	17.24	0	90.28	28	203.425	7.2652	13.36	0	87.79
Blocks	2	0.24873	0.124364	15.32	0	5.73	2	11.588	5.7941	10.65	0	5.00
Linear	6	2.73001	0.455001	56.06	0	62.89	6	155.739	25.9565	47.72	0	67.21
Spindle Speed	2	1.3213	0.660649	81.4	0	30.44	2	75.679	37.8395	69.57	0	32.66
Feed rate	2	0.02099	0.010495	1.29	0.283	0.48	2	13.169	6.5843	12.11	0	5.68
Coating	2	1.38772	0.693859	85.49	0	31.97	2	66.891	33.4457	61.49	0	28.87
2-Way Interactions	12	0.87894	0.073245	9.02	0	20.25	12	24.008	2.0007	3.68	0.001	10.36
Spindle speed x Feed rate	4	0.17284	0.043211	5.32	0.001	3.98	4	4.185	1.0462	1.92	0.12	1.81
Spindle speed x Coating	4	0.6936	0.1734	21.36	0	15.98	4	17.554	4.3885	8.07	0	7.58
Feed rate x Coating	4	0.01249	0.003122	0.38	0.819	0.29	4	2.269	0.5673	1.04	0.394	0.98
3-Way Interactions	8	0.06116	0.007645	0.94	0.491	1.41	8	12.09	1.5112	2.78	0.012	5.22
Spindle speed x Feed rate x Coating	8	0.06116	0.007645	0.94	0.491	1.41	8	12.09	1.5112	2.78	0.012	5.22
Error	52	0.42205	0.008116			9.72	52	28.282	0.5439			12.21
Total	80	4.34088				100	80	231.708				100

DF: Total degrees of freedom, Adjs SS: Adjusted Sum of Squares, Adj MS: Adjusted Mean of Squares. F-Value: a ratio of two variances, P-Value: Probability.

Table 5: ANOVA table showing the percentage contribution of cutting parameters and cutting tool coating effect on burr parameters

	Burr height at entrance						Burr height at exit					
Source	**DF**	**Adj SS**	**Adj MS**	**F-Value**	**P-Value**	**%**	**DF**	**Adj SS**	**Adj MS**	**F-Value**	**P-Value**	**Percentage contribution**
Model	28	858.922	30.676	26.99	0	93.56	28	21775	777.68	124.53	0	98.53
Blocks	2	8.573	4.286	3.77	0.03	0.93	2	25.3	12.67	2.03	0.142	0.11
Linear	6	290.515	48.419	42.61	0	31.65	6	17698.6	2949.77	472.33	0	80.09
Spindle Speed	2	51.093	25.547	22.48	0	5.57	2	1310.2	655.11	104.9	0	5.93
Feed rate	2	207.59	103.795	91.34	0	22.61	2	593.8	296.89	47.54	0	2.69
Coating	2	31.831	15.916	14.01	0	3.47	2	15794.6	7897.29	1264.56	0	71.47
2-Way Interactions	12	470.937	39.245	34.53	0	51.30	12	2960.4	246.7	39.5	0	13.40
Spindle speed x Feed rate	4	230.706	57.677	50.75	0	25.13	4	422.2	105.55	16.9	0	1.91
Spindle speed x Coating	4	118.157	29.539	25.99	0	12.87	4	507.2	126.81	20.31	0	2.30
Feed rate x Coating	4	122.073	30.518	26.85	0	13.30	4	2030.9	507.73	81.3	0	9.19
3-Way Interactions	8	88.898	11.112	9.78	0	9.68	8	1090.7	136.33	21.83	0	4.94
Spindle speed x Feed rate x Coating	8	88.898	11.112	9.78	0	9.68	8	1090.7	136.33	21.83	0	4.94
Error	52	59.093	1.136			6.44	52	324.7	6.25			1.47
Total	80	918.016				100	80	22099.7				100
	Burr root thickness at entrance						**Burr root thickness at exit**					
Source	**DF**	**Adj SS**	**Adj MS**	**F-Value**	**P-Value**	**%**	**DF**	**Adj SS**	**Adj MS**	**F-Value**	**P-Value**	**Percentage contribution**
Model	28	0.018379	0.000656	26.85	0	93.53	28	0.063314	0.002261	70.36	0	97.43
Blocks	2	0.000009	0.000004	0.18	0.838	0.05	2	0.000002	0.000001	0.03	0.971	0.00
Linear	6	0.007051	0.001175	48.08	0	35.88	6	0.053246	0.008874	276.13	0	81.94
Spindle Speed	2	0.000828	0.000414	16.94	0	4.21	2	0.002984	0.001492	46.42	0	4.59
Feed rate	2	0.002435	0.001217	49.81	0	12.39	2	0.009765	0.004882	151.91	0	15.03
Coating	2	0.003788	0.001894	77.49	0	19.28	2	0.040498	0.020249	630.04	0	62.32
2-Way Interactions	12	0.006207	0.000517	21.16	0	31.59	12	0.006962	0.00058	18.05	0	10.71
Spindle speed x Feed rate	4	0.003577	0.000894	36.58	0	18.20	4	0.001953	0.000488	15.19	0	3.01
Spindle speed x Coating	4	0.002102	0.000525	21.5	0	10.70	4	0.002718	0.000679	21.14	0	4.18
Feed rate x Coating	4	0.000528	0.000132	5.41	0.001	2.69	4	0.002292	0.000573	17.83	0	3.53
3-Way Interactions	8	0.005112	0.000639	26.14	0	26.02	8	0.003103	0.000388	12.07	0	4.77
Spindle speed x Feed rate x Coating	8	0.005112	0.000639	26.14	0	26.02	8	0.003103	0.000388	12.07	0	4.77
Error	52	0.001271	0.000024			6.47	52	0.001671	0.000032			2.57
Total	80	0.01965				100	80	0.064985				100

DF: Total degrees of freedom, Adjs SS: Adjusted Sum of Squares, Adj MS: Adjusted Mean of Squares. F-Value: a ratio of two variances, P-Value: Probability.